ELSEVIER

NDT&E International 33 (2000) 33–41

NDT&E international

www.elsevier.com/locate/ndteint

Wave propagation in thin Plexiglas plates: implications for Rayleigh waves

A. Zerwer[a], M.A. Polak[a,*], J.C. Santamarina[b]

[a]*Department of Civil Engineering, University of Waterloo, 200 University Ave. West, Waterloo, ON, Canada*
[b]*Department of Civil and Environmental Engineering, Georgia Institute of Technology, Atlanta, GA, USA*

Received 15 July 1998; received in revised form 20 February 1999; accepted 24 February 1999

Abstract

Two-dimensional (2D) experimental models are often used to study wave propagation problems. The advantages of using 2D experimental models, as opposed to 3D models, is the reduction of both extraneous reflections and mathematical complexity. Further, many structural elements conform to this geometry. The following study examines Rayleigh wave motion in thin Plexiglas sheets. Source–receiver time domain measurements were made at different locations on the Plexiglas sheet. The time–distance space was 2D-Fourier transformed into the frequency–wavenumber space to facilitate the analysis of wave modes propagating in the Plexiglas sheet. Experimental results showed that fundamental symmetric (S_0) and antisymmetric (A_0) Lamb waves propagated through the plate. Along the thickness of the plate, a non-dispersive Rayleigh wave was generated. Lamb waves were found to interfere with the Rayleigh wave. The assumption of generalized plane stress is preserved if higher mode Lamb waves have low energy content. © 1999 Elsevier Science Ltd. All rights reserved.

Keywords: Rayleigh waves; Lamb waves; Dispersion; Plates

1. Introduction

Wave-based techniques play a central role in non-destructive characterization of existing infrastructure. Transmission measurements provide average information about the body. Further, transmission measurements with various illumination angles can be tomographically inverted to infer the spatial distribution of material parameters within the body, such as slowness or attenuation. However, the spatial coverage and the wavefront directionality renders tomographic imaging ineffective near the surface of the structural element [1]. Yet, damage tends to initiate and to concentrate at the surface. For the study of surface imperfections and slots, Rayleigh waves that form and propagate along boundaries, are better suited than body waves.

The study reported herein was designed to develop the appropriate test procedures, signal processing algorithms and interpretation criteria needed for the characterization, with Rayleigh waves, of steel and concrete structural elements, such as beams, columns and slabs. Specifically, the effects of two-dimensional (2D) boundary conditions on the applicability, accuracy and limitations, of representing three-dimensional (3D) Rayleigh wave based studies, are explored.

This paper starts with a brief introduction to the relevant theoretical aspects of wave propagation in plates. Test procedures employed for time domain measurements and signal processing techniques used to analyze the acquired data are described. Finally, a description of the observed plate mode vibrations is given and discussed with respect to the generation of a non-dispersive Rayleigh wave.

2. Theory

Wave propagation studies in 2D models often involve plates held in the upright position (Fig. 1). An impact applied to the edge of the plate generates compression, shear and Rayleigh waves that propagate along the plate edge. To ensure minimal out-of-plane motion, the wavelength of the propagating oscillations should be much larger than the plate thickness [2,3].

Oliver et al. [2] used the concept of generalized plane stress to simulate 3D motion in a 2D model. By maintaining a thin plate in the upright position and assuming the wavelengths propagating through the plate were long compared to the plate thickness (ratio of 1/10), the compression wave could be considered non-dispersive. Laboratory experimentation

* Corresponding author. Tel.: + 1-519-888-4567; fax: + 1-519-888-6197.

0963-8695/00/$ - see front matter © 1999 Elsevier Science Ltd. All rights reserved.
PII: S0963-8695(99)00010-9

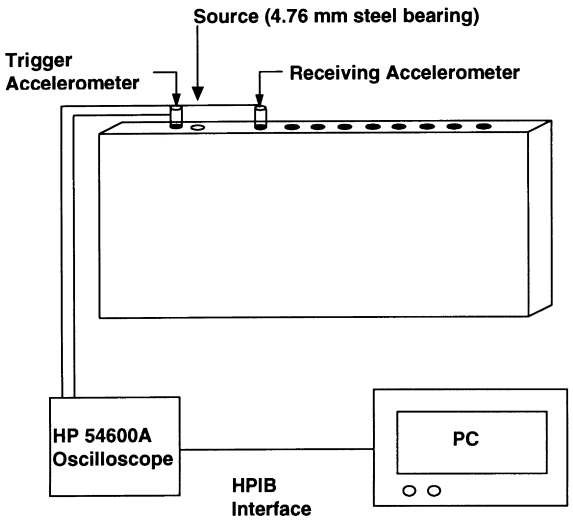

Fig. 1. Schematic diagram of experimental configuration.

by Parham and Sutton [4] verified the long wavelength assumption by illustrating the dispersive nature of the compression wave as the plate thickness was altered. However, as shown in the following equations, the compression wave velocity in a plate is slower than in an infinite body

$$V_{\mathrm{p}}^{\mathrm{body}} = \sqrt{\frac{E(1-\nu)}{\rho(1+\nu)(1-2\nu)}}, \tag{1a}$$

$$V_{\mathrm{p}}^{\mathrm{plate}} = \sqrt{\frac{E}{\rho(1-\nu^2)}}, \tag{1b}$$

where the velocity is a function of density, given by ρ, Young's modulus, E and Poisson's ratio, ν. As will be discussed in a later section, the compression wave is a fundamental symmetric Lamb wave that exhibits minimal dispersion at low frequencies.

The vertical shear wave velocity, polarized within the plane of the plate, remains unchanged between the 3D and the 2D cases. The propagation of a non-dispersive compression wave and a shear wave allows for the generation of a non-dispersive Rayleigh wave along the edge of the plate. The Rayleigh wave velocity (V_{R}) can be calculated by using the 2D compression wave velocity in the Rayleigh wave equation,

$$\left(2 - \frac{V_{\mathrm{R}}^2}{V_{\mathrm{s}}^2}\right)^2 = 4\sqrt{1 - \frac{V_{\mathrm{R}}^2}{V_{\mathrm{p}}^2}}\sqrt{1 - \frac{V_{\mathrm{R}}^2}{V_{\mathrm{s}}^2}} \tag{2}$$

where V_{p} is the compression wave velocity calculated using Eq. (1b), and V_{s} is the shear wave velocity. For Plexiglas, the compressional body wave velocity is 2700 m/s and the shear wave velocity is 1370 m/s. When using the generalized plane stress approximation [5], the 2D compression wave velocity becomes 2360 m/s. By solving Eq. (2), the calculated Rayleigh wave velocity becomes 1280 m/s.

Another important feature of wave propagation in 2D models is the propagation of a fundamental antisymmetric Lamb wave (A_0) through the 2D model [2]. The Lamb wave motion in plates is described by the Rayleigh–Lamb frequency equation. The interaction of compression and shear waves at two parallel, traction free, boundaries was used to develop a general frequency equation for plates, first derived by Rayleigh [6] and by Lamb [7]

$$\frac{\tan \beta b}{\tan \alpha b} + \left\{\frac{4\alpha\beta k^2}{(k^2-\beta^2)^2}\right\}^{\pm 1} = 0, \tag{3}$$

where

$$\alpha^2 = \frac{\omega^2}{V_{\mathrm{p}}^2} - k^2, \qquad \beta^2 = \frac{\omega^2}{V_{\mathrm{s}}^2} - k^2$$

b is half the plate thickness, k is the wavenumber, ω is the circular frequency, V_{p} and V_{s} are the compression and shear wave velocities, respectively. Symmetric and antisymmetric components are obtained by changing the exponent to $+1$ or -1 respectively.

The Rayleigh–Lamb frequency equation incorporates the Rayleigh wave, the Lamb wave, and the classical plate flexural motion [8–10]. Propagating Lamb wave modes present in a plate are dependent on the compression and shear wave velocities, and the frequency/wavelength content of the wave. In general, for thin plates, fundamental symmetric (S_0) and antisymmetric (A_0) Lamb modes are present. Higher mode symmetric and antisymmetric Lamb waves are formed at increasing frequencies. Further, as an extension of the Rayleigh–Lamb frequency equation, reflections of Lamb waves from surfaces with mixed boundary conditions can create an infinite number of harmonics associated with each of the propagating Lamb modes [11].

In summary, three propagation modes are sought: S_0 which corresponds to the propagation of compression waves, the A_0 mode and the Rayleigh wave. Given the proximity to side and bottom boundaries, multiple reflections should be expected.

3. Test procedure

A sheet of Plexiglas with dimensions of 1220 × 300 × 6 mm^3 was held in the upright position as shown in Fig. 1. The source was a 4.76 mm (3/16 in.) diameter steel bearing, dropped through a glass tube from a height of 50 mm, onto the edge of the Plexiglas sheet. The vertical acceleration history at different points on the edge of the plate was measured with an accelerometer coupled onto the plate edge with beeswax. Time domain traces were recorded with an oscilloscope and transferred to a computer for analysis. Another accelerometer mounted 3 mm behind the source was used as a trigger.

The source was placed 200 mm (8 in.) from the plate edge as shown in Fig. 1. The accelerometer was moved to

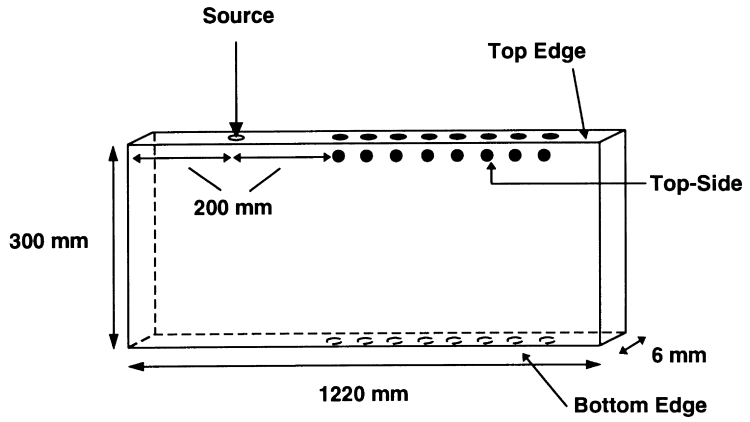

(a)

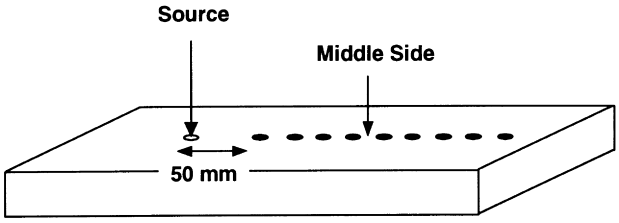

(b)

Fig. 2. Time domain measurements were made with the plate in an upright and flatlying position.

different positions along the top-edge, top-side, and bottom-edge of the plate as shown in Fig. 2(a). Positions were spaced at 12.7 mm (1/2 in.) intervals for a total length of 508 mm (20 in.) giving 41 traces for all tests. A separate set of measurements was made along the middle side of the plate. In this test, the impact was applied to the side of a flatlying plate supported on foam, as shown in Fig. 2(b).

4. Signal processing

Two-dimensional frequency analysis was used to calculate the dispersion curves measured on the Plexiglas sheet. A matrix **T** was assembled with the time series data. Each column in the matrix corresponds to a measurement. Therefore the $\mathbf{T}_{ij}$ element is the ith value for the jth measurement. The ordering of the measurements in **T** reflects the spatial arrangement in the field, i.e. neighboring columns correspond to neighboring measurements [12,13]. Each time domain signal, downloaded from the oscilloscope, had 1000 data points with a sampling frequency of 1 MHz. The entire time domain trace was used without windowing any reflections. The time domain signals were zero-tail packed to 2000 points and the spatial domain was zero-tail packed to 201 points. Therefore, the size of matrix **T** is 2000×201. To reduce frequency and wavenumber leakage, a Hamming window was applied across the spatial and temporal directions of the matrix. The matrix **T** was 2D Fourier transformed to determine spatial and temporal frequencies. The magnitude of each complex element in the transformed matrix **F** was calculated. The data were presented as a contour plot of amplitude in the frequency–wavenumber space. Vibrational modes in the contour plot are identified as a sequence of peaks. The phase velocity of the different vibrational modes can be calculated by dividing the frequency by the wavenumber of the corresponding peak [9]

$$V_{\text{phase}} = \frac{\lambda}{\mathrm{T}} = \frac{\omega}{k}, \tag{4}$$

where

$$k = \frac{2\pi}{\lambda} \qquad \text{and} \qquad \omega = \frac{2\pi}{\mathrm{T}}.$$

Note that only the frequency–wavenumber location of peaks are needed for phase velocity calculations.

5. Source characteristics

Several initial measurements were completed to determine the frequency range that renders high coherence; this ensures linear behavior and proper signal to noise ratio.

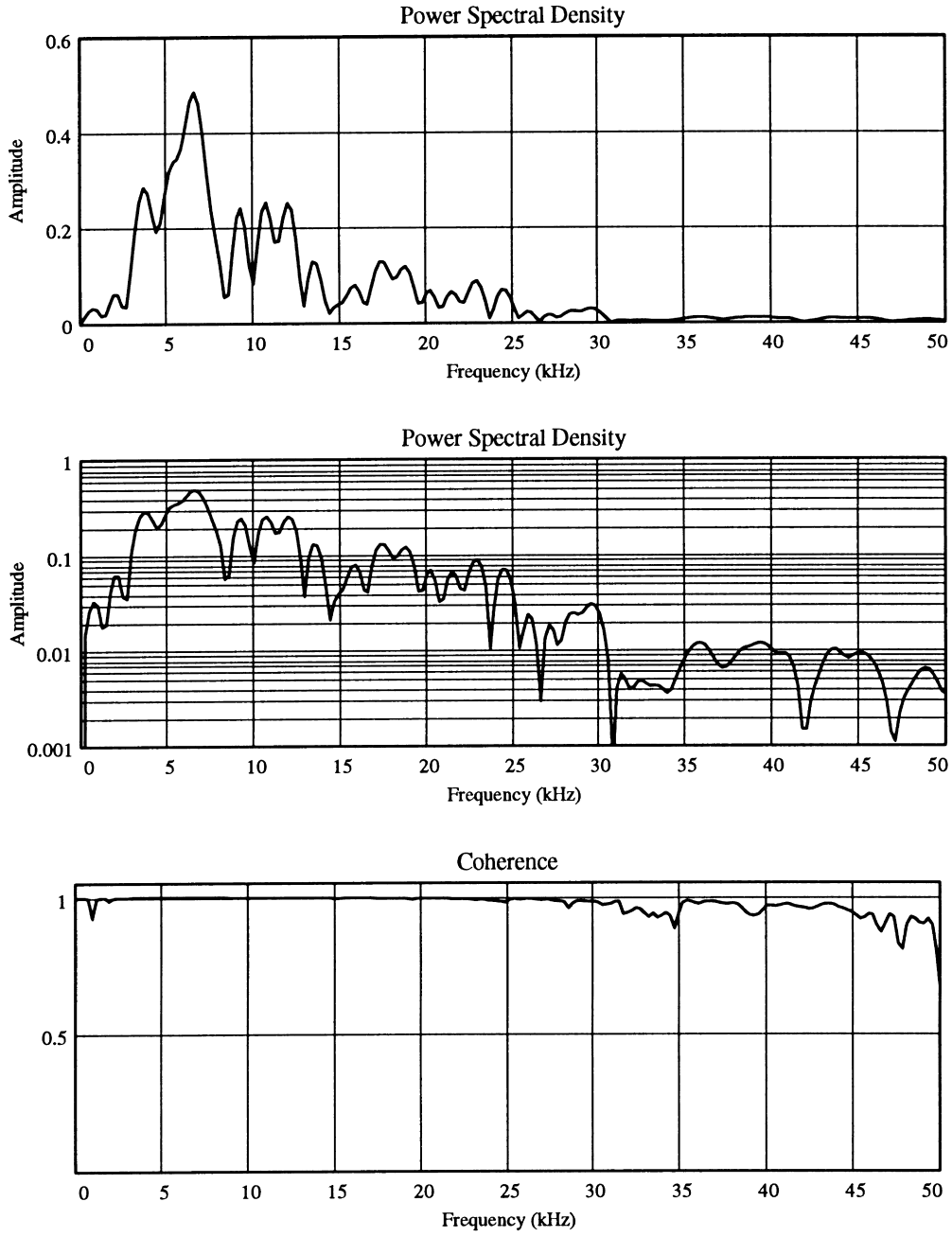

Fig. 3. Power spectrum density and coherence function of the source.

Coherence is computed as

$$\gamma^2(\omega) = \frac{\bar{G}_{yx}\bar{G}^*_{yx}}{\bar{G}_{xx}\bar{G}_{yy}}, \tag{5}$$

where the bar denotes average of multiple similarly measured signals and $*$ indicates the complex conjugate. The cross spectral densities are G_{yx} and G_{xy} and the auto spectral densities are G_{xx} and G_{yy}. Perfect coherence between two receivers is obtained when $\gamma^2 = 1$.

The steel bearing was dropped onto the edge of the Plexiglas plate at a distance of 152 mm from the centerline of the sheet. Two sets of 20 measurements were made with the receiving accelerometer mounted at 50 mm on either side of the centerline. Coherence calculations were made between the two sets of receiver measurements.

Results are shown in Fig. 3. The main energy band was between 2 and 30 kHz. High coherence values were computed in this band ($\gamma^2 \cong 1$). Reduced coherence values were found at low frequencies, suggesting the inability of the source to produce long wavelengths.

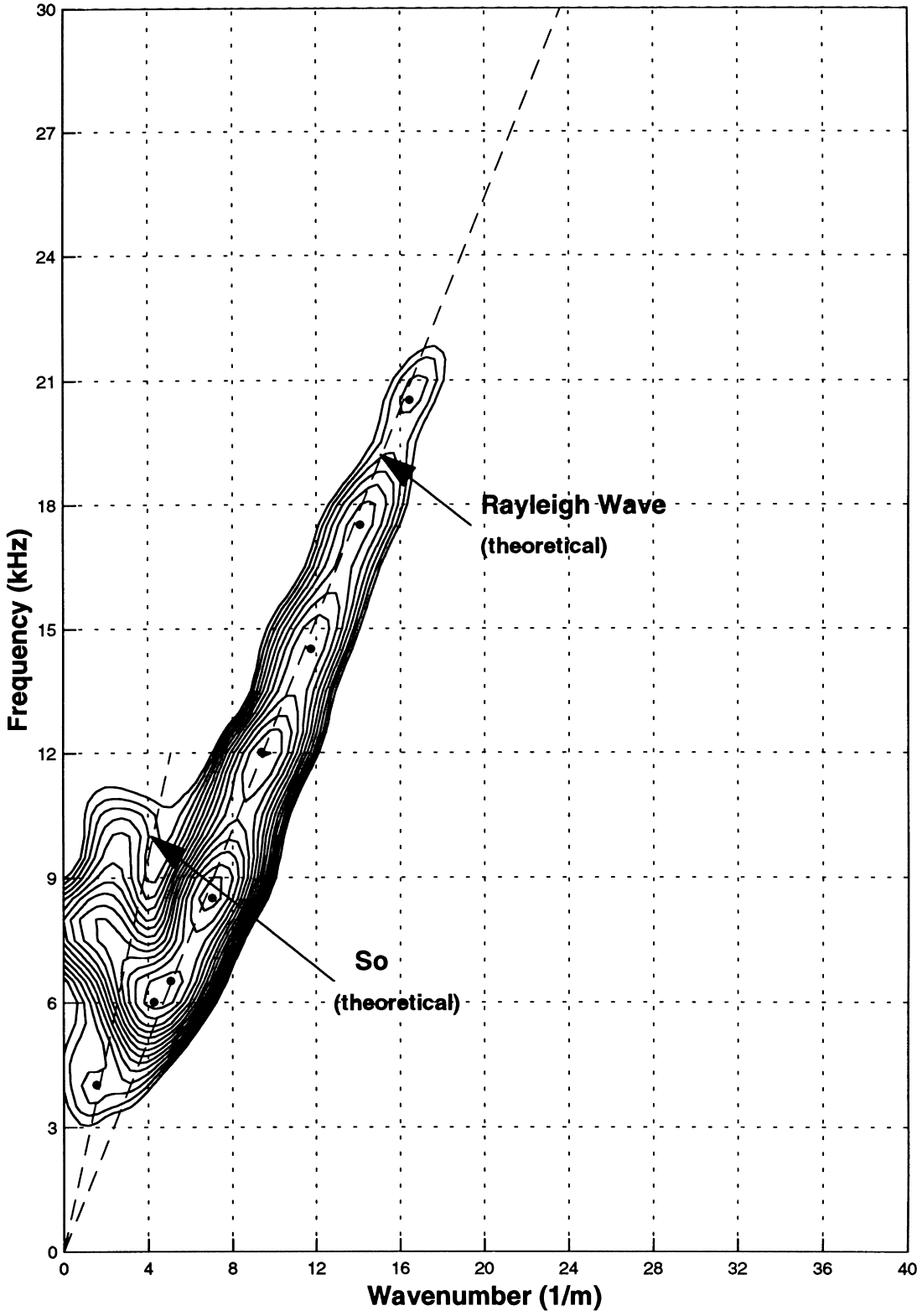

Fig. 4. Dispersion of Rayleigh wave on the top-edge of the plate (setup in Fig. 2a).

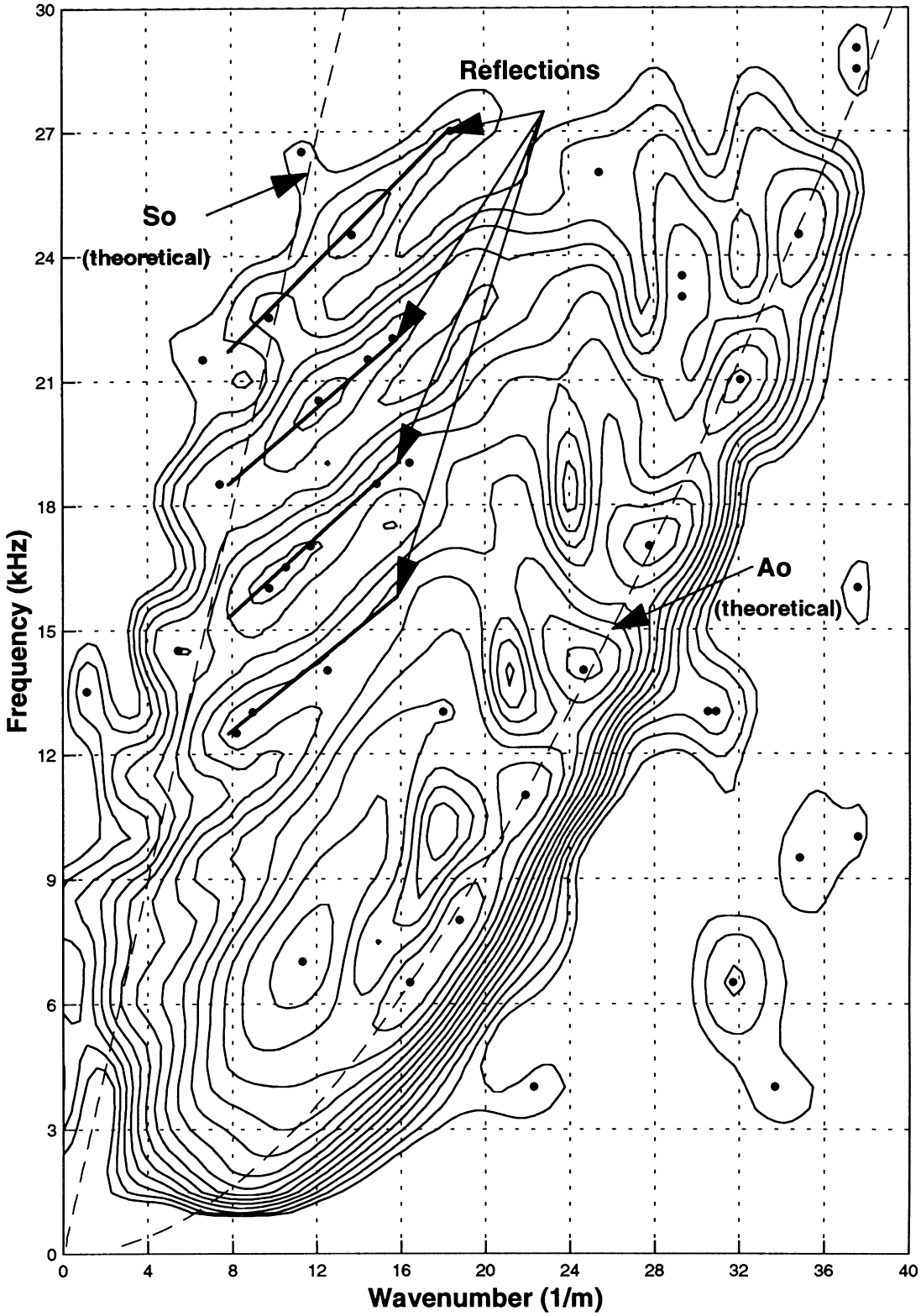

Fig. 5. Fundamental Lamb modes measured along the middle side of the plate (setup in Fig. 2b). The S_0 wave is not clearly visible due to reflections of the A_0 wave.

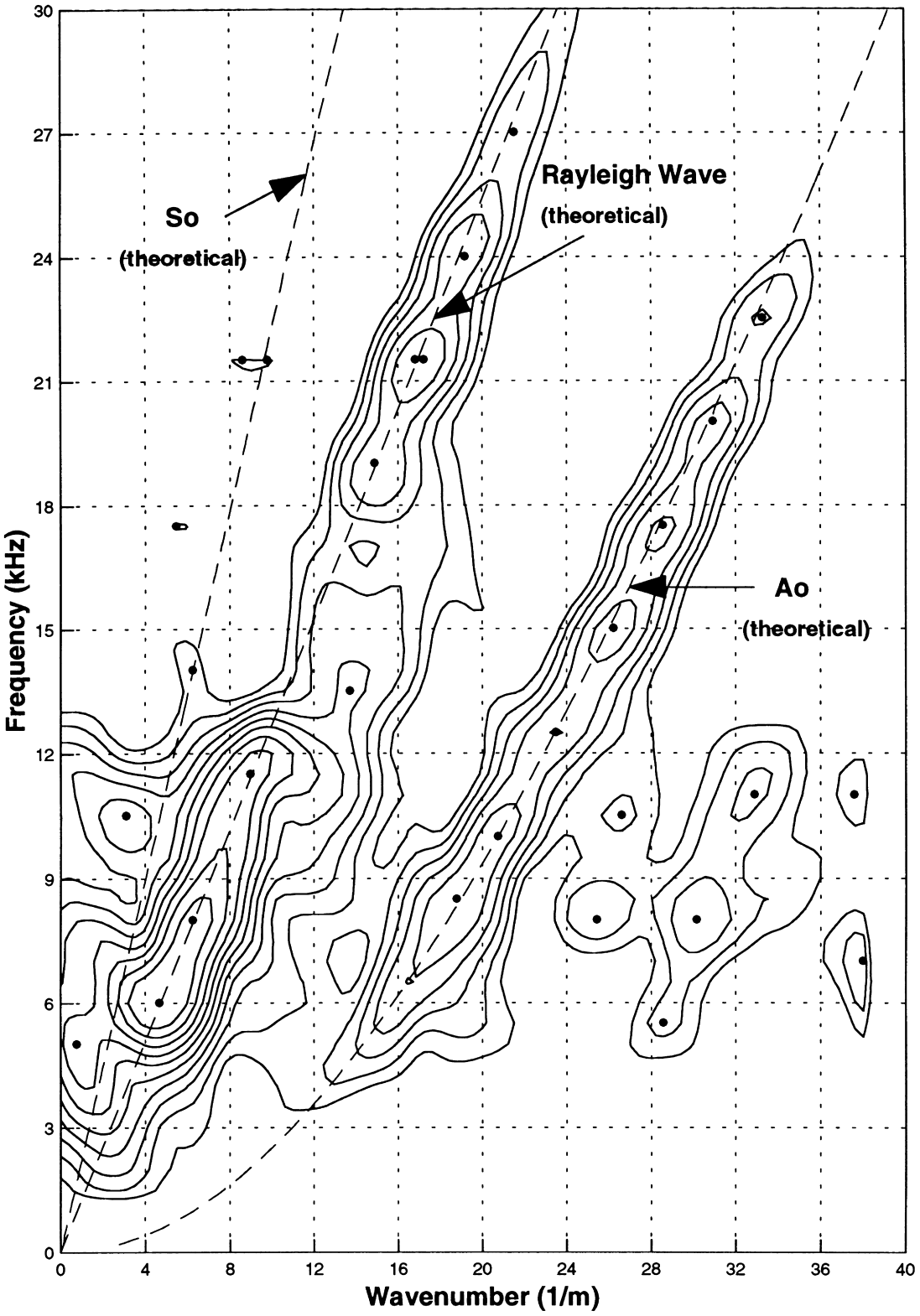

Fig. 6. Measurement of the Rayleigh wave and A_0 mode along the top-side of the plate.

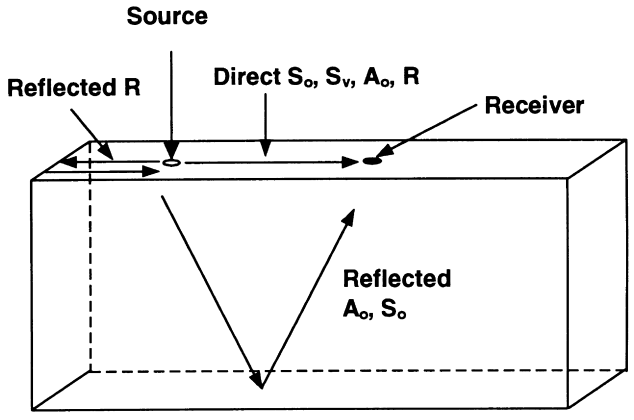

(a)

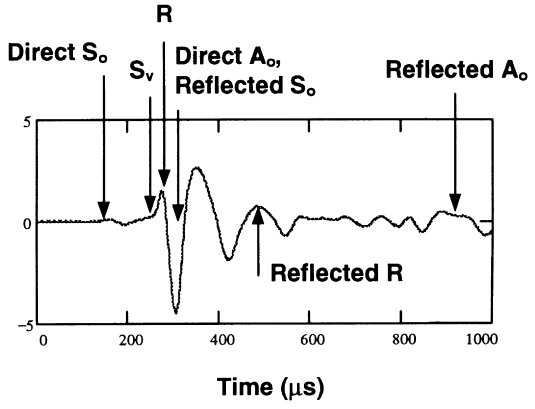

(b)

Fig. 7. Typical time domain traces measured on the plate.

6. Observations

In all of the following frequency–wavenumber contour plots experimental peaks are identified by the solid circles. Theoretically calculated phase velocities are shown as a dashed line:

Top-edge. The contour plot of the 2D Fourier transform of signals measured on the top surface of the Plexiglas sheet are shown in Fig. 4. The phase velocity calculated from the main trend line of the peaks is 1276 m/s, which compares well with the Rayleigh wave velocity of 1280 m/s determined from theoretical calculations. The main energy band of the Rayleigh wave is consistent with the frequency range where high coherence is expected from the source.

The high velocity peaks measured at low frequency and wavenumber correspond to the compression (S_0) wave. The S_0 mode is weak, having only one peak at a low wavenumber.

Middle side. The results for measurements made along the middle side of the plate (Fig. 2(b)) are shown in Fig. 5. The A_0 mode, as well as reflections of the A_0 mode from the sides of the plate, are clearly visible. Similar to Fig. 4, the fundamental symmetric mode is weak, but appears to cover a wider frequency–wavenumber range.

Top-side. Dispersion measurements obtained along the top lateral side of the plate, while applying the source along the top-edge (Fig. 2(a)), are shown in Fig. 6. Both the Rayleigh wave and the A_0 wave are visible. The low energy of the Rayleigh wave dispersion curve, between 12–18 kHz, corresponds to the high energy components of the A_0 mode. Conversely, high energy components of the Rayleigh wave corresponds to low energy in the A_0 mode.

Bottom-edge. A final set of measurements were made on the bottom-edge of the sheet while applying the source along the top-edge (Fig. 2(a)). A weak Rayleigh wave mode was found propagating along the bottom-edge of the sheet. Additional higher velocity modes were also observed. A distinct dispersion relation was not evident.

7. Discussion and closing remarks

Measured phase velocities were compared to theoretically predicted phase velocities to identify the different propagating modes. As shown in Figs. 4 and 6, the Rayleigh wave velocity calculated using Eq. (2) (dashed lined) compares well with the measured peaks. Close agreement was likewise obtained between the measured (peaks) and calculated (dashed line) fundamental Lamb wave phase velocities also shown in Figs. 5 and 6. Theoretical phase velocities for the S_0 and A_0 modes were calculated using Eq. (3). The phase velocity calculated for the S_0 wave agrees well with the velocity calculated for the compression wave using Eq. (2). As shown in Figs. 5 and 6, the phase velocity for the S_0 wave shows no dispersion at low frequencies (long wavelengths). Calculations using Eq. (3) illustrates that the S_0 dispersion curve remains flat up to higher frequencies as the wavelength becomes shorter, which is in accordance with the results obtained by Parham and Sutton [4].

The measured velocities for the different modes permit computing the travel times for the different wavefronts. Consider the case when the receiver is 200 mm away from the source along the top-edge (Fig. 7(a)). The measured time domain signal is shown in Fig. 7(b). Arrows indicate the times computed for the different arrivals.

An important consideration is the effect of the A_0 wave on the Rayleigh wave propagating along the top-edge of the Plexiglas plate. As shown in Fig. 6, the Rayleigh wave and the antisymmetric Lamb wave are observed. Within the frequency ranges of these measurements (0–30 kHz), the velocity of the A_0 wave increases to the point where it is superposed onto the motion of the Rayleigh wave. The result is that the initial portion of the time domain trace for the Rayleigh wave can be compared to the three dimensional motion of a Rayleigh wave, however, the final portion will be a combination of a Rayleigh and an A_0 wave (Fig. 7(b)). Results in Fig. 4 indicate that the A_0 wave does not

appear to affect the main energy band of the Rayleigh wave measured along the top-edge specimens.

The presented results have implications for the implementation of numerical models and forward simulations. A plate can be represented with either generalized plane stress or plane strain conditions. Generalized plane stress conditions exist in the plane parallel to the two main dimensions of the plate (Fig. 2(a)). Plane strain conditions prevail through the plate thickness, in the direction of the two main dimensions of the plate, away from the edges (Fig. 2(b), short wavelengths).

From a wave propagation perspective, the generalized plane stress model implies that only the fundamental Lamb modes are present through the thickness of the plate. As was discussed by Kane and Mindlin [14], coupling between higher Lamb modes cannot be incorporated into the generalized plane stress condition. From the measurements made on the Plexiglas plate, higher mode Lamb waves were not observed, however, reflections of the A_0 mode were measured. The presence of the A_0 mode and associated reflections, did not appear to affect the Rayleigh wave.

Acknowledgements

This study is part of a NDT research project with the application to structural elements. Support has been provided by NSERC (Natural Sciences and Engineering Council Canada), OGS (Ontario Graduate Scholarship), MDC Geological Consultants and Turkstra Lumber.

References

[1] Santamarina JC, Fratta D. Introduction to signals and inverse problems in civil engineering. New York: ASCE, 1998.
[2] Oliver H, Press F, Ewing M. Two-dimensional model seismology. Geophysics 1954;19:202–19.
[3] O'Brien PNS, Symes MP. Model seismology. Reports on Progress in Physics 1971;34:697–764.
[4] Parham RT, Sutton DJ. The transition between 2 and 3-dimensional waves in seismic models. Bull Seis Soc Am 1971;61(4):957–60.
[5] Love AEH. A treatise on the theory of elasticity. 4. New York: Dover, 1927.
[6] Lord Rayleigh. On the free vibrations of an infinite plate of homogeneous isotropic matter. Proc Lond Math Soc 1888;20:225.
[7] Lamb H. On waves in an elastic plate. Proc Lond Math Soc 1889;21:85.
[8] Yu Yi-Yuan. Vibrations of elastic plates. New York: Springer, 1996.
[9] Graff KF. Wave motion in elastic solids. New York: Dover, 1975.
[10] Achenbach JD. Wave propagation in elastic solids. North Holland: Amsterdam, 1973.
[11] Mindlin RD. Waves and vibrations in isotropic, elastic plates. In: Goodier JN, Hoff N, editors. Structural mechanics, 1960. p. 199.
[12] Alleyne D, Cawley P. A two-dimensional Fourier transform method for the measurement of propagating multimode signals. J Acous Soc Am 1991;89(3):1159–68.
[13] Costley Jr. RD, Berthelot YH. Dispersion curve analysis of laser-generated Lamb waves. Ultrasonics 1994;32:249–53.
[14] Kane TR, Mindlin RD. High-frequency extensional vibrations of plates. J Appl Mech 1956;23:277–83.